Proceedings of the 22nd National and 11th International ISHMT-ASME Heat and Mass Transfer Conference

December 28-31, 2013, IIT Kharagpur, India

HMTC1300104

ENERGY EFFICIENCY OF SWEEPING GAS MEMBRANE DISTILLATION DESALINATION CYCLES

Jaichander Swaminathan, John H. Lienhard V*
Rohsenow Kendall Heat Transfer Laboratory
Department of Mechanical Engineering
Massachusetts Institute of Technology
Cambridge, MA 02139-4307, USA

ABSTRACT

Sweeping Gas Membrane Distillation (SGMD) is a carrier gas membrane distillation technology that can use low temperature, low grade and waste heat sources and is well suited to small scale desalination systems. Understanding the overall thermal efficiency, usually in the form of a Gained Output Ratio (GOR), is an important step its towards commercial implementation. This article presents a 'one dimensional' numerical model of the heat and mass transfer processes in a flat sheet SGMD module coupled to a multistage bubble column dehumidifier (MSBCDH). The model is validated against flux data reported in literature. It is used to analyze entropy generation and study the effect of various parameters on the efficiency of SGMD desalination cycles. Entropy generation in both the SGMD module and the dehumidifier can be important and they both affect the overall cycle efficiency. GOR values in excess of 2.5 are observed in single stage once through SGMD-MSBCDH desalination cycles.

NOMENCLATURE

B	membrane distillation coefficient [kg/m^2 s Pa]
c_p	specific heat at constant pressure [J/kgK]
d	channel depth [m]
dA	area element [m^2]
dz	elemental length [m]
h	specific enthalpy [J/kg]
h_{fg}	enthalpy of vaporization [J/kg]
J	mass flux [kg/m^2 s]
k_{mass}	mass transfer coefficient [m/s]
L	module effective length [m]
$\dot{m}$	mass flow rate [kg/s]
$\dot{m}_{\text{r}}$	air water mass flow rate ratio [-]
MW	molecular weight [kg/kmol]
n_{cells}	number of computational cells [-]
P	pressure [Pa]
p	partial pressure[Pa]
q	heat flux [W/m^2]
$\dot{Q}$	rate of heat addition [W]
s	specific entropy [J/kg K]
sal	salinity [g/kg]
$\dot{S}_{\text{gen}}$	entropy generation rate [W/K]
$\dot{s}_{\text{gen}}$	specific entropy generation [J/kg K]
T	temperature [°C]
v	velocity [m/s]
w	module width [m]
x	mole fraction [-]
z	distance along module length [m]
α	heat transfer coefficient [W/m^2 K]
ω	humidity ratio [kg/kg]
δ	thickness of membrane [m]
ρ	density [kg/m^3]
$(\cdot)_{\text{a}}$	air
$(\cdot)_{\text{b}}$	bulk/free stream
$(\cdot)_{\text{c}}$	coolant
$(\cdot)_{\text{da}}$	dry air

*Corresponding Author: lienhard@mit.edu

$(\cdot)_{\text{eff}}$	effective
$(\cdot)_{\text{f}}$	feed
$(\cdot)_{\text{in}}$	inlet
$(\cdot)_{\text{m}}$	membrane
$(\cdot)_{\text{out}}$	outlet
$(\cdot)_{\text{p}}$	permeate
$(\cdot)_{\text{sg}}$	sweeping gas
$(\cdot)_{\text{v}}$	vapor
$(\cdot)_{\text{wb}}$	wet bulb
AGMD	Air Gap Membrane Distillation
BCDH	Bubble Column Dehumidifier
DCMD	Direct Contact Membrane Distillation
DBT	Dry Bulb Temperature [°C]
EES	Engineering Equation Solver
GOR	Gained Output Ratio [-]
MD	Membrane Distillation
MSBCDH	Multistage Bubble Column Dehumidifier
SGMD	Sweeping Gas Membrane Distillation
VMD	Vacuum Membrane Distillation
MD	Membrane Distillation
MED	Multiple Effect Distillation
MSF	Multiple Stage Flash
TTD	Terminal Temperature Difference [°C]

1 INTRODUCTION

In membrane distillation (MD), desalination is achieved by passing water vapor through the pores of a hydrophobic membrane by establishing a temperature-driven vapor pressure difference between the feed and permeate sides of the module. The hydrophobicity of the membrane ensures that liquid water does not pass through and thereby ensures almost 100% elimination of non-volatile impurities such as salt in the permeate. Hot saline water constitutes the feed in these systems. Based on the design of the permeate side, MD processes have been classified into four major categories - Direct Contact (DC), Air Gap (AG), Sweeping Gas (SG), and Vacuum (V) MD. [1]

DCMD has a cold pure water stream flowing counter-current to the feed on the permeate side, onto which the vapor condenses immediately after crossing the membrane. Since the hot and cold streams are separated only by a thin membrane, there is significant sensible heat transfer. This heat transfer, in addition to being a loss, also adds to temperature polarization in the streams [2]. AGMD on the other hand has a cold condensing plate separated from the membrane by a thin layer of stagnant air. This way, sensible heat loss from the feed is reduced since air has a lower thermal conductivity. The evaporated water has to diffuse through the air gap and reach the film of condensate on the cold plate which becomes one of the rate limiting steps. SGMD has an air stream that flows on the permeate side picking up the incoming vapor and getting humidified as it moves along the module. Generally the temperature of air also increases along the module.

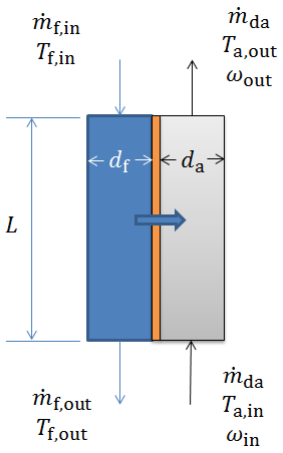

FIGURE 1. SCHEMATIC DIAGRAM OF SGMD PROCESS

The hot humid air is then cooled in a condenser where product water is recovered. Though SGMD combines advantages of both DCMD (lower mass transfer resistance on the permeate side) and AGMD (lower sensible heat loss across the membrane) configurations, since additional equipment (dehumidifier) is required to condense the product water out of the air stream, it has received scant attention compared to other types of MD technology, both in theoretical and experimental studies [3]. Until 2011, only 4.5% of papers related to MD were on SGMD [4].

With the development of compact, high-effectiveness and low cost dehumidifiers [5], SGMD has the become more competitive as a means to purify water. Most literature on MD has focused on improving membrane flux rather than on energy efficiency (GOR), which is the relevant parameter for comparison with other established thermal desalination technologies such as MSF and MED [6]. Therefore, in this study, we develop a numerical model of the heat and mass transfer processes within a SGMD module, which is then coupled with a dehumidifier model to form a complete desalination system for efficiency analysis.

1.1 SGMD process

Figure 1 shows a schematic diagram of the SGMD module. The feed stream and the air stream flow counter-current to each other. The feed inlet temperature is of the order of $T_{\text{f,in}} \approx 60°\text{C}$. The air stream generally enters at a lower temperature of about $T_{\text{a,in}} \approx 25°\text{C}$. Both heat and mass are transferred from the hot feed side to the air stream. The temperature and humidity of the air stream increase along the module whereas the feed cools down before exiting.

The driving force for heat transfer is the difference in temperature (dry bulb temperature - DBT, for the air stream) between the stream. Mass transfer is driven by the vapor partial pressure difference between the liquid surface and the air stream.

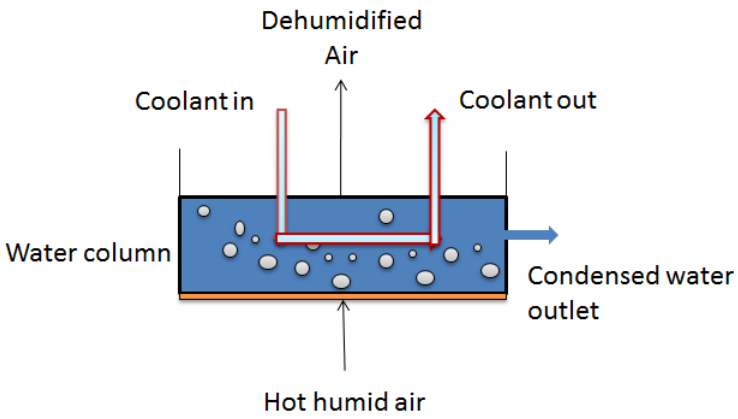

FIGURE 2. SCHEMATIC OF BCDH PROCESS

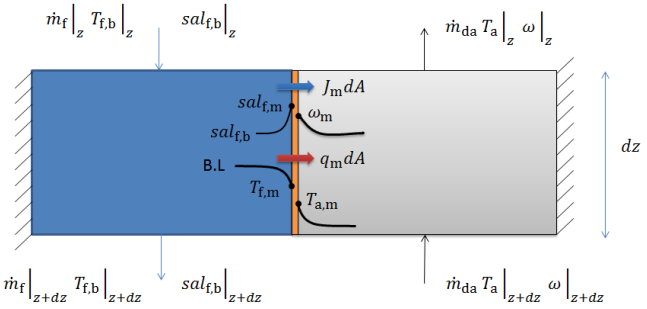

FIGURE 3. SGMD COMPUTATIONAL CELL WITH HEAT AND MASS FLUXES AND ASSOCIATED BOUNDARY LAYERS

1.2 Bubble column dehumidifier (BCDH) process

In this study we use a multistage bubble column dehumidifier (MSBCDH) as the dehumidifier along with the SGMD module to complete the desalination cycle. MSBCDH has been proposed as an alternative to conventional dehumidifiers that use large metal areas for condensation and are therefore quite expensive. Figure 2 shows a schematic diagram of a single stage BCDH. The BCDH is an example of a direct contact dehumidifier where a hot moist air stream is bubbled through a column of pure water. The water vapor from the air bubbles condenses at the bubble surface and releases energy into the water column. By the time the air leaves the water column, it is cooled down and leaves close to the temperature of the water column. The heat released by the condensing vapor is removed from the water column by a coolant stream. In our system, the inlet saline feed water flowing inside a copper tube acts as the coolant. The energy released by condensation is therefore recovered and reused for preheating the feed water. Further discussion on the performance of BCDH compared to conventional dehumidifiers and the effect of high proportion of non-condensible gases is available in [5].

In Sec. 2, the modeling methodology is explained, followed by validation of the model in Sec. 3. Sec. 4 has a brief discussion on entropy generation within the individual components. Finally, results from simulations of the complete desalination cycle are discussed in Sec. 5.

2 MODELING

The numerical modeling was carried out using the commercial software, Engineering Equation Solver (EES) [7]. EES is an iterative numerical simultaneous eqution solver that uses accurate thermodynamic property data for air-water mixtures and water. The air-water mixture properties in EES are evaluated using formulae presented by Hyland and Wexer [8] and water properties are evaluated using the IAPWS 1995 formulation [9].

2.1 SGMD module

Method Khayet et al. [10, 11] have developed theoretical models of the transport processes within a SGMD module by considering the resistances to heat transfer, namely the feed and air side boundary layers as well as the membrane. Charfi et al. [12] modeled the module in two dimensions using the Navier-Stokes equation for both fluid streams with a suitable coupled boundary conditions at the membrane interfaces.

The modeling approach followed in this work is an extension of the technique presented in [6] for AGMD, DCMD and VMD systems. A one dimensional modeling approach is followed wherein property variations along the length direction are modeled using suitable conservation equations. The fluid streams are assumed uniform in the width direction. Along the depth direction the effect of the boundary layers close to the membrane surface for either stream can not be ignored. These effects are captured by solving for the fluid properties at the membrane interface for both streams, and the interface values are also allowed to vary along the flow direction (length) of the module.

The advantage of this method is that it is computationally less cumbersome compared to a 2D Navier Stokes model. At the same time there is enough detail available to draw useful conclusions about system performance and to study the effect of various system variables.

Equations Along the feed flow direction, the MD module is discretized into small control volumes of size dz, where $dz = L/n_{\text{cells}}$. The transport processes within and around one

such section are shown in Fig. 3.

The main MD flux is modeled using a membrane property called the flux coefficient, B which is given by Eq. 1. B is considered constant for a particular system. For a particular membrane material, the value of B could vary under different operating conditions. The units of B are kg/m^2 s Pa.

$$J_{\mathrm{m}} = B \times (p_{\mathrm{v,f,m}} - p_{\mathrm{v,a,m}}) \tag{1}$$

The feed side partial pressure of water vapor is the saturation vapor pressure over the liquid interface and is therefore only a function of liquid temperature and local salinity as given by Raolt's law:

$$p_{\mathrm{v,f,m}} = P_{\mathrm{sat}}(T_{\mathrm{f,m}})\, x_{\mathrm{f,m}} \tag{2}$$

On the air side, we use the ideal gas relationships to obtain $p_{\mathrm{v,a,m}}$ as shown in Eq. 3 and 4:

$$p_{\mathrm{v,a,m}} = P_{\mathrm{a}} x_{\mathrm{a,m}} \tag{3}$$

$$x_{\mathrm{a,m}} = \frac{\frac{\omega_{\mathrm{m}}}{MW_{\mathrm{v}}}}{\frac{\omega_{\mathrm{m}}}{MW_{\mathrm{v}}} + \frac{1}{MW_{\mathrm{a}}}} \tag{4}$$

We see that while on the feed side the vapor pressure is a strong function of temperature, on the air side, temperature of the air stream doesn't come into the picture. Most SGMD models [10] assume that the air stream is saturated at the inlet and remains saturated subsequently. Under those conditions, the partial pressure of water vapor in the air gap side is also only a function of the air temperature, since the state of saturated air is completely determined by its temperature. In our model, we do not make this assumption and hence in general, the partial pressure is not just a function of air's DBT.

On the feed side, mass and energy balance equations (Eq. 5,6) are solved:

$$\dot{m}_{\mathrm{f}}|_{z+dz} = \dot{m}_{\mathrm{f}}|_{z} - J_{\mathrm{m}} dA \tag{5}$$

$$(\dot{m}_{\mathrm{f}} h_{\mathrm{f,b}})\,|_{z+dz} = (\dot{m}_{\mathrm{f}} h_{\mathrm{f,b}})\,|_{z} - (J_m h_{\mathrm{v,f,m}} + q_{\mathrm{m}})\, dA \tag{6}$$

Theoretically, for an internal flow Eq. 6 is valid only for bulk temperature defined as a mass averaged temperature over the cross sectional area of the flow. Here the equation is used with the value of the temperature outside the boundary layer as an approximation of the theoretical bulk value.

In addition to the mass flux, there is a heat flux across the membrane governed by the temperature difference across the membrane and the effective thermal conductivity of the MD membrane:

$$q_{\mathrm{m}} = \frac{k_{\mathrm{eff,m}}}{\delta_{\mathrm{m}}} (T_{\mathrm{f,m}} - T_{\mathrm{a,m}}) \tag{7}$$

The value of temperature at the membrane interfaces is determined as a function of the net heat transfer, heat transfer coefficient and free stream temperature value (Eq. 8, 9):

$$T_{\mathrm{f,m}} = T_{\mathrm{f,b}} - (J_{\mathrm{m}}(h_{\mathrm{v,f,m}} - h_{\mathrm{f,b}}) + q_{\mathrm{m}})/\alpha_{\mathrm{f}} \tag{8}$$

Note that while the entire energy loss from the feed side contributes to the temperature polarization on the feed side, only the sensible heat addition to the air stream is considered for temperature polarization on the air side. The latent heat of evaporation does not feature in the temperature polarization expression. Even under fogging conditions where a small amount of liquid water is formed in the air stream, the condensation and corresponding energy release is assumed to happen in the bulk since relative humidity computed at the membrane interface is always less than 1. The excess thermal energy carried by the vapor and the sensible heat input are transferred into the vapor stream from the membrane interface by convection:

$$T_{\mathrm{a,m}} = T_{\mathrm{a}} + (J_{\mathrm{m}}\, c_{p,\mathrm{v}} (T_{\mathrm{f,m}} - T_{\mathrm{a}})) + q_{\mathrm{m}})/\alpha_{\mathrm{a}} \tag{9}$$

The heat and mass transfer coefficients are evaluated using standard correlations for Nu and Sh for internal flows based on the Re, Pr and Sc numbers of the flow [13].

The salinity at the membrane interface on the feed side is evaluated using the film model of concentration polarization as

$$sal_{\mathrm{f,m}} = sal_{\mathrm{f,b}}\, exp\left(\frac{J_{\mathrm{m}}}{k_{\mathrm{mass,f}}\, \rho_{\mathrm{f}}}\right) \tag{10}$$

Air Stream In Eq. 4, we saw that the vapor partial pressure depends on the humidity ratio at the membrane interface. This is evaluated again using the film model as

$$\frac{\rho\left(\frac{1}{1+\omega}\right)}{\rho_m\left(\frac{1}{1+\omega_m}\right)} = exp\left(\frac{J_{\mathrm{m}}}{k_{\mathrm{mass,a}}\,\rho_{\mathrm{a}}}\right) \tag{11}$$

Mass and energy balance equations are solved on the air gap side as well:

$$\dot{m}_{\mathrm{da}}\left(\omega|_z - \omega|_{z+dz}\right) = J_{\mathrm{m}} dA \tag{12}$$

$$\dot{m}_{\mathrm{da}}(h_{\mathrm{a}}|_z - h_{\mathrm{a}}|_{z+dz}) = J_{\mathrm{m}} h_{\mathrm{v,f,m}} dA + q_{\mathrm{m}} dA \tag{13}$$

When EES solves the above equations based on the mass and energy fluxes that enter the air stream, since the air-water mixture enthalpy function in EES is defined even for supersaturated states (relative humidity > 1), a check needs to be placed on whether supersaturation occurs. Whenever the air stream tends to become supersatured with water, the state of air is forced back to the saturation line at the same enthalpy in order to simulate fogging. Any excess water after this is done, is assumed to be in the liquid state as fog carried forward by the air stream.

The local entropy generation for the control volume located between z and $z+dz$ is evaluated to make sure that the second law of thermodynamics is satisfied everywhere locally.

2.2 Multistage bubble column dehumidifier

Figure 4 shows a schematic diagram of a multistage bubble column dehumidifier. Hot moist air is bubbled through a series of water columns (stages), which are cooled by cool feed water. The condensed moisture from each stage is added to a subsequent stage and finally water at the lowest temperature (from stage 1) is extracted as pure product. Air leaves saturated at a temperature close to the that of the water column in each stage in a well designed BCDH. The water stream also gets heated to a temperature slightly below the temperature of water column. This is illustrated in Fig. 5. The difference in temperature between the air and coolant that leave a stage is called the terminal temperature difference (TTD) of the stage.

The main goal of the present study is to model the SGMD module in detail. Tow and Lienhard [14] have reported data from several bubble column dehumidifier experiments. Based on that data, a TTD of 1 °C is assumed for each stage of a well designed MSBCDH. In addition to this imposed condition, first law and mass conservation are solved for each stage and the stages are coupled together in order to solve for the overall outputs of the dehumidifier.

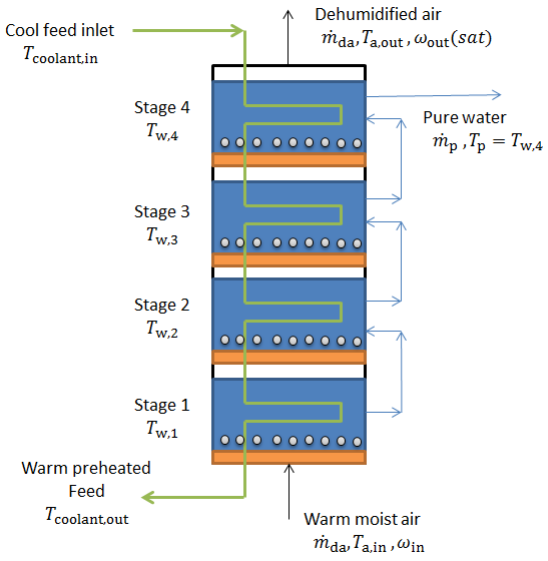

FIGURE 4. SCHEMATIC DIAGRAM OF MSBCDH SYSTEM WITH 4 STAGES

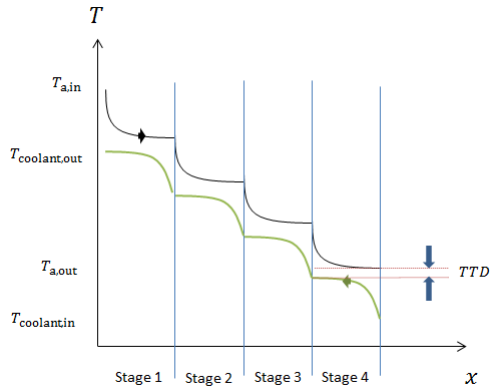

FIGURE 5. TEMPERATURE VS POSITION FOR A MSBCDH SYSTEM SHOWING THE TERMINAL TEMPERATURE DIFFERENCE (TTD)

3 VALIDATION

Charfi et al. [12] have published flux data from experiments conducted on a flat sheet SGMD module. Based on the data reported, the geometry of the experimental setup is estimated and programmed into the one dimensional model.

While the physical properties of the membrane such as porosity, mean pore size, and tortuosity have been reported, no value of membrane distillation mass transfer coefficient B is mentioned. The B value was fixed at 1.7×10^{-7} kg/m^2 s Pa a good match between the 1D model simulation results and exper-

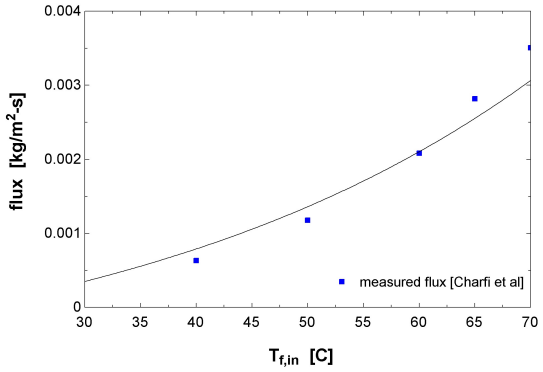

FIGURE 6. FLUX VS TEMPERATURE OF FEED INLET COMPARED WITH EXPERIMENTAL DATA

TABLE 1. BASELINE VALUES FOR VALIDATION TEST CASES

S No	Variable	Value	Units
1	$T_{\mathrm{f,in}}$	50	°C
2	$T_{\mathrm{a,in}}$	20	°C
3	v_{f}	0.15	m/s
4	v_{a}	0.8	m/s
5	sal_{in}	0	ppt
6	L	0.068	m
7	w	0.08235	m
8	$d_{\mathrm{f}}, d_{\mathrm{a}}$	0.005	m
9	B	1.7×10^{-7}	kg/m^2 s Pa

imental data is obtained. (Fig. 6).

Though additional experimental measurements are not included in the reference, simulation results from the 2D model are discussed. The overall match between experiment and the simulation has also been reported to be quite good ($R^2 = 0.9406$). The baseline conditions of their experiments and important physical parameters are collected in Tab. 1. Similar simulations are carried out using the one dimensional model described here.

The corresponding results from our model, at the same value of B determined earlier are included in Fig. 7. The flux decreases with an increase in air temperature since the inlet air stream was maintained at a saturated state in the experiment. As a result, an increase in temperature of the air meant a corresponding exponential increase in vapor partial pressure in the air and hence a reduction in the net driving force for mass transfer.

The SGMD flux increases with an increase in air stream velocity (Fig. 7(b)) since a higher air mass flow rate implies quicker vapor removal by the air stream. At very low air mass flow rates, the air stream is effectively humidified and heated close to the temperature of the feed, at which point mass transfer driving force becomes very small. Under such conditions, if the air mass flow is increased, the outlet state of air will not change much. Net permeate production for the module is evaluated as

$$\dot{m}_{\mathrm{p}} = \dot{m}_{\mathrm{da}}(\omega_{\mathrm{out}} - \omega_{\mathrm{in}}) \tag{14}$$

While $\omega_{\mathrm{out}} \approx \omega_{\mathrm{sat}}(T = T_{\mathrm{f,in}})$ doesn't change much, the increase in $\dot{m}_{\mathrm{da}}$ would lead to a linear increase in flux. As the velocity increases however, the transport processes within the module will not be able to keep up and heat the air up to it's maximum value. As a result the rate of increase in flux drops with further increase in v_{a}. At higher velocities, the heat and mass transfer coefficients are also higher which results in lower difference in temperature and concentration across the boundary layers. In other words, the temperature and concentration polarization are reduced, contributing to an increase in flux.

The velocity of the feed has a smaller impact on flux. The flux increases with increase in v_f is owing to the reduction in temperature and concentration polarization in the feed channel.

Comparing with corresponding graphs from the 2D model (Fig. 5,7,8 of [12]), we see that the trends predicted by the two dimensional model are captured accurately by the present model. The absolute value of flux differs between the two models by a maximum of about 20%.

4 SGMD & MSBCDH SYSTEM ANALYSIS

4.1 Entropy generation and GOR

The efficiency of a thermal desalination cycle is given by the Gained Output Ratio (GOR), a measure of the extent to which the supplied heat energy is reused within the system for evaporation and purification of the feed. GOR is defined as

$$GOR = \frac{\dot{m}_{\mathrm{p}} h_{fg}}{\dot{Q}_{\mathrm{in}}} \tag{15}$$

In this paper, h_{fg} for GOR evaluation is taken at 25°C since MD uses low grade, low temperature heat sources. Other publications may use the value of h_{fg} at 100°C. Since $h_{fg}(100°C) = 2.257 \times 10^6$ J/kg and $h_{fg}(100°C) = 2.442 \times 10^6$ J/kg, a GOR of 2.6 reported here would correspond to GOR=2.8 if enthalpy of vaporization at T_{bp} is used.

For desalination systems, it has been shown that minimizing specific entropy generation ($\dot{s}_{\mathrm{gen}}$ - entropy generated per unit rate

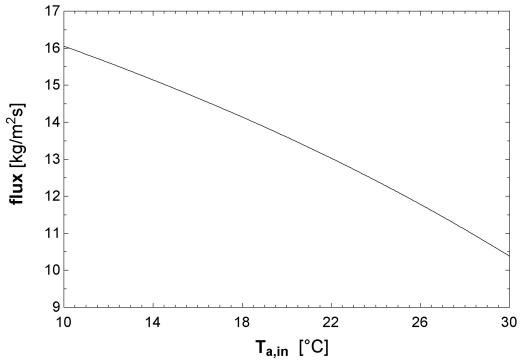

(a) Effect of saturated air inlet temperature

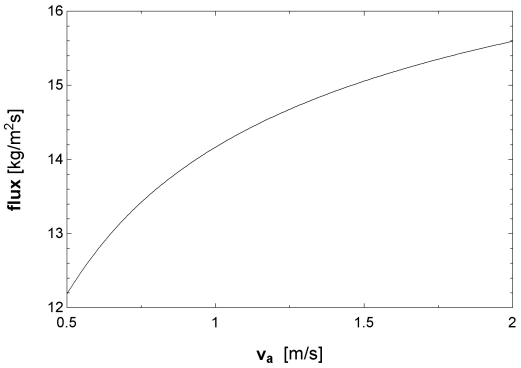

(b) Effect of air stream velocity

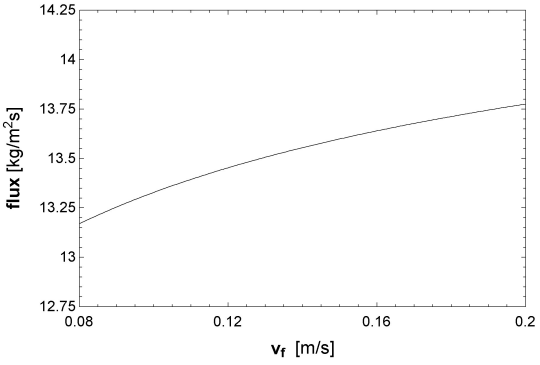

(c) Effect of feed velocity

FIGURE 7. FLUX PREDICTION

of permeate production) results in maximum GOR [15]. The entropy generation characteristics of the SGMD and MSBCDH systems are analyzed separately before they are put together to form a complete desalination system.

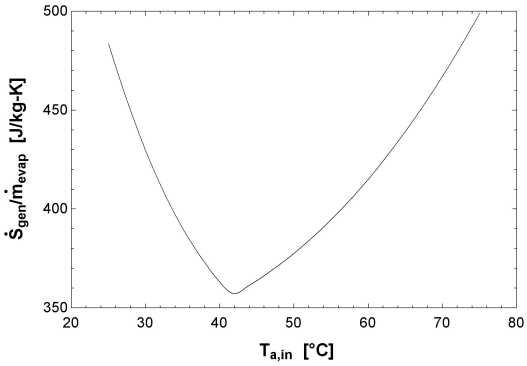

FIGURE 8. SPECIFIC ENTROPY GENERATION AS A FUNCTION OF INLET AIR TEMPERATURE. HUMIDITY = $\omega_{\mathrm{sat}}(25^{\circ}C)$

4.2 SGMD module

As noted earlier, in this modeling framework, the air stream is not constrained to be saturated at all times. Instead, the air state can evolve as dictated by the actual heat and mass transfer driving forces. This enables us to analyze the effect of air stream preheating on entropy generation in the SGMD module. When the air stream is heated at constant total pressure, on a psychrometric chart, the state of air is displaced horizontally towards the right since there is no change in humidity ratio. Since the humidity ratio remains constant, the partial pressure of water vapor in in the air stream does not change. Therefore, while the mass transfer process is largely unaffected (except for secondary influences), the heat transfer between the streams is reduced. This would therefore lead to reduced entropy generation in the SGMD module.

Figure 8 shows this effect. The entropy generation within the module reduces and increases again with increase in inlet air DBT. The rate of decrease in entropy generation is very steep because of air state hitting the saturation dome and fogging occurring within the stream. The process path traced by the sweeping gas in the case of two inlet air temperatures (40,50°C) is depicted on a psychrometic chart in Fig. 9. In Fig.9(a), the air stream gets heated and humidified until it hits the saturation dome. Thereafter, as discussed in Sec. 2.1, the air state is manually forced to follow the saturation dome. Total specific enthalpy of the air is used to choose the point along the saturation line. A small amount of liquid water is formed whose enthalpy is ignored while determining the air state ($h_{\mathrm{v}} \gg h_{\mathrm{l}}$), but the quantity of liquid water/fog is calculated and carried forward along with the air stream.

In Fig. 9(b) on the other hand, the air is seen to be almost exclusively humidified(the state of the air stream evolves vertically upward). Initially the air loses DBT as some heat transfer occurs to the water stream which is at a lower temperature. In

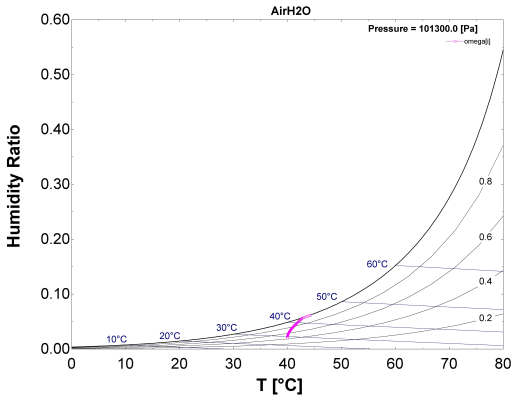

(a) Air inlet temperature = 40°C

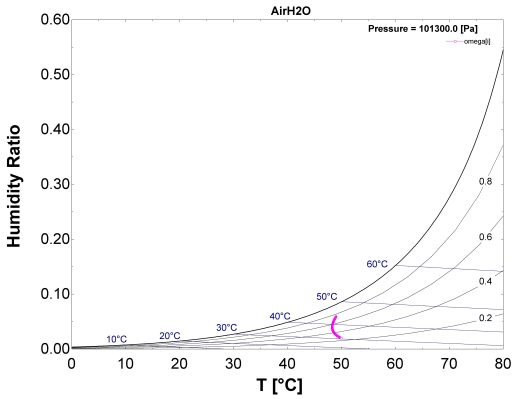

(b) Air inlet temperature = 50°C

FIGURE 9. AIR STREAM STATE

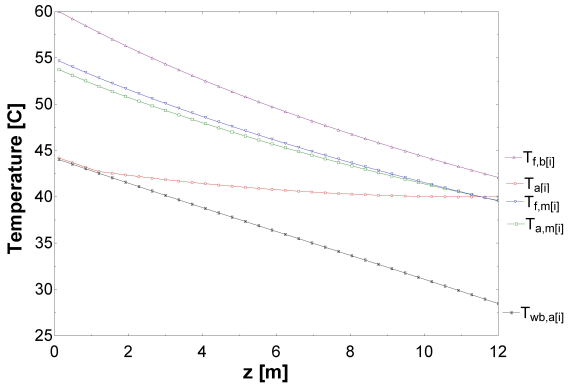

(a) Air inlet temperature = 40°C

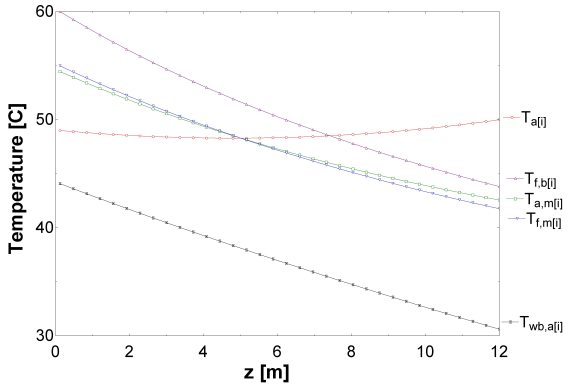

(b) Air inlet temperature= 50°C

FIGURE 10. TEMPERATURE VS. POSITION

the latter part of the of module, the air is heated and humidified by the feed stream.

The flow evolution along the length of the module can be visualized better using the help of a temperature vs. position plot. In Fig. 10(a), we see that the water DBT denoted by T_a does not vary much initially as it flows from L=12m to about 2m. At this point, the air stream becomes saturated and it starts following the saturation curve with $T_a = T_{wb}$. On the other hand, in Fig. 10(b), while the DBT does not change over the length of the module, the wet bulb temperature increases steadily.

In both the graphs, the temperatures of the air and feed at the membrane interface are almost equal. This shows that there is significant temperature polarization in both streams. Another effect of this is that there is very little sensible heat transfer from the feed to sweeping gas ($q_m \approx 30-40$ W/m^2). Any sensible heat transfer, in MD is considered a loss. Interestingly, while the high air side temperature polarization adds a thermal resistance within the stream, it is beneficial in reducing the net sensible heat loss from the feed.

Figure 11 shows the vapor pressure difference across the membrane which drives transfer of pure water vapor. As explained earlier, the increased DBT of the inlet air does not affect the vapor pressure of the air stream and hence the mass transfer processes in the two cases are nearly identical. In Fig. 11(b), we see that in the lower specific entropy production case, the air stream vapor pressure at the exit is slightly higher indicating a small increase in overall flux. These graphs characterize the physical processes within the module and help confirm that the model captures the phenomena accurately.

4.3 Multistage bubble column dehumidifier

The specific entropy generation in the proposed MSBCDH model is plotted in Fig. 12. As expected, the specific entropy generation has a minima with respect to changing $\dot{m}_{da}$ with other parameters fixed. Combined heat and mass transfer devices such as dehumidifiers (and humidifiers) produce minimum entropy when the heat capacity rates of the two streams are matched [16] .

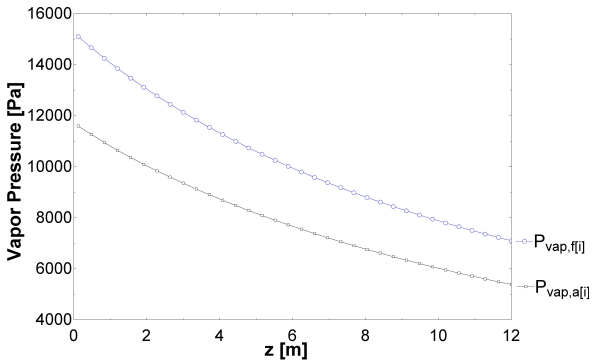

(a) Air inlet temperature = 40°C

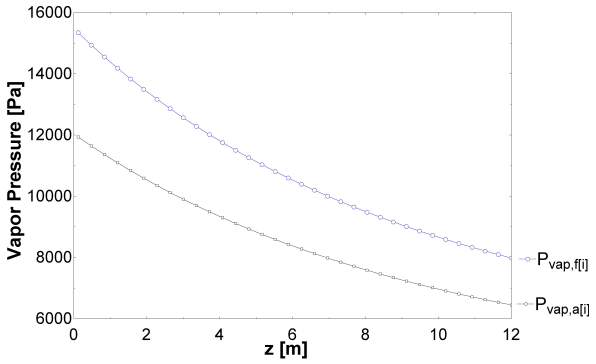

(b) Air inlet temperature = 50°C

FIGURE 11. VAPOR PRESSURE VS. POSITION

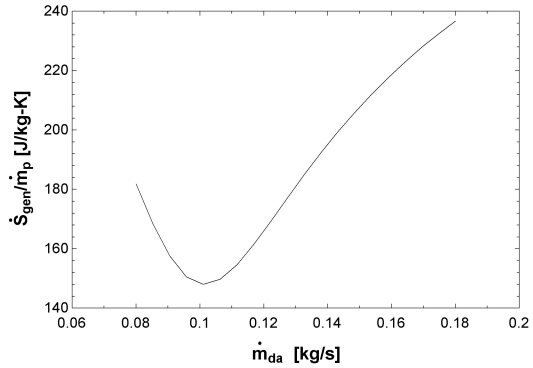

(a) Effect of $\dot{m}_{da}$

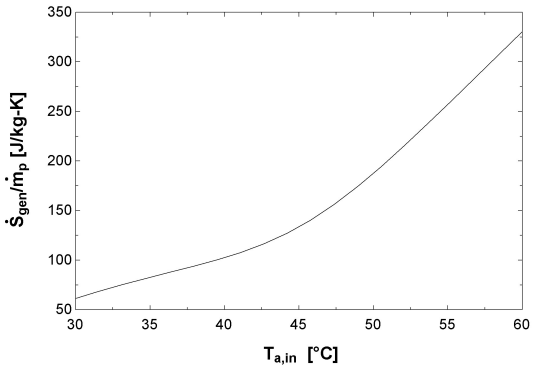

(b) Effect of $T_{a,in,BCDH}$

FIGURE 12. SPECIFIC ENTROPY GENERATION IN A MSBCDH. ($T_{\mathrm{a,in}}$ = 50°C, $\dot{m}_{\mathrm{c}}$= 0.189 kg/s, $T_{\mathrm{c,in}}$= 25°C)

The irreversibility within the device increases with increase in $T_{\mathrm{a,in,BCDH}}$ under these conditions (12(b)). This is expected since with an increase in inlet air temperature, both heat and mass transfer driving forces increase in the system.

5 CYCLE ANALYSIS

A schematic diagram of the overall desalination cycle is illustrated in Fig. 13. The two models are combined by matching their inlet and outlet states suitably in EES. The configuration chosen is a closed air open water configuration. Cold water is taken into the dehumidifier and used to as the coolant. As it passes through, the enthalpy of condensation is transferred from the water column into the cold water stream and it is preheated. The feed water then goes through a water heater where it is heated to the cycle top temperature. In this study, the cycle top temperature is fixed and hence the heat input varies depending on the extent of preheating. The hot water then goes through the SGMD module. Here evaporation causes cooling of the feed. The minimum temperature to which the feed can get cooled is the wet bulb temperature of the air inlet into the SGMD module and as it approaches this temperature the driving force for mass transfer will reduce. The brine that exits the SGMD module is disposed.

The air stream forms a closed loop as the name of the configuration indicates. Air enters the SGMD module and is humidified by addition of vapor from the feed stream. In the process, the temperature of the air also increases. This stream is then taken into the MSBCDH where it is bubbled through multiple water baths using spargers. As the bubbles rise, air is cooled and excess water vapor condenses into the water. The air that exits the MSBCDH is then fed back into the SGMD module.

Since the two devices are now coupled, the number of degrees of freedom is reduced. The temperature of the air stream is no longer an input to the system. The mass of the liquid streams are also equal in both the devices. We previously observed that s_{gen} is minimized in the MSBCDH at a particular value of $m_{\mathrm{r}} = \dot{m}_{\mathrm{da}}/\dot{m}_{\mathrm{f}}$. Similarly the SGMD system would produce minimum entropy at a different value of m_{r}. Since the entropy generation in both devices is of the same order of magni-

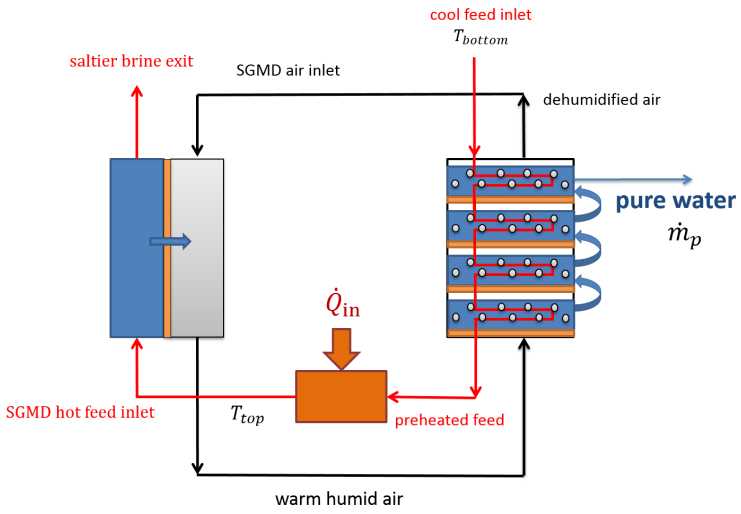

FIGURE 13. COMPLETE SGMD-MSBCDH DESALINATION SYSTEM

tude, the overall system performance and the effect of the system inputs would be a result of the combined effect of both devices.

The baseline parameters for the simulations are given in Tab. 2. Each of the parameters are varied around their baseline value keeping the other variables constant to understand their effect on the overall cycle GOR.

5.1 Mass flow rates

The mass flow rates are important parameters in the SGMD desalination system. With both the SGMD module and the MSBCDH irreversibilities being functions of m_{r}, the overall system too is very sensitive to the mass flow rates of feed and air. In addition to its effect on the thermodynamics as described above, the mass flow rate of a stream also affects the Reynolds number and thereby the Nusselt and Sherwood number of the stream in the SGMD module. Through its effect on the Nu and Sh, an increase in mass flow rate of either stream would lead to a monotonic increase in GOR of the cycle. The thermodynamic effect dominates as is seen in Fig. 14, with the GOR attaining a maximum at a particular value of feed and air mass flow rate and reducing thereafter.

5.2 Temperatures

SGMD feed inlet The temperature of the feed input the SGMD module is a design variable and is the cycle's top temperature. Figure 15 shows the effect of cycle top temperature on GOR. When all other parameters such as system geometry and flow rates are fixed, GOR is maximized at $T_{\text{f,in}} = 70^{\circ}\text{C}$.

TABLE 2. BASELINE VALUES OF SGMD DESALINATION SYSTEM

S No	Variable	Value	Units
1	$T_{\text{f,in}}$	60	°C
2	$T_{\text{cold,w,in}}$	25	°C
3	$\dot{m}_{\text{f,in}}$	0.189	kg/s
4	$\dot{m}_{\text{da}}$	0.1345	kg/s
5	$sal_{\text{f,in}}$	30	ppt
6	L	12	m
7	w	0.125	m
8	d_{f}	0.004	m
9	d_{a}	0.04	m
10	B	16×10^{-7}	kg/m^2 s Pa
11	TTD	1	°C
12	$n_{\text{BCDH,stages}}$	6	-

Coolant The temperature of the coolant (feed inlet from the environment) has a smaller effect on GOR (Fig. 16). Since the baseline mass flow rates were chosen such that GOR is maximized, the GOR is maximum close to $T_{\text{c,in}} = 25^{\circ}\text{C}$.

5.3 Geometry

Geometry of the SGMD module affects the transport processes within significantly. Figure 17 shows the influence of the effective length and width of the module on GOR. Both length and width affect the total available membrane area. While the length does not affect the cross section and hence the flow velocity, changing the width introduces these additional effects as well. At the baseline operating parameters and module dimensions (chosen to be in the range of other commonly studied MD systems [6]), the SGMD module design is not optimized since $T_{\text{f,out}}$ from the module is much higher than the wet bulb temperature of the air inlet (see Fig. 10, for example). Increasing the area of the membrane is similar to increasing the area of a heat exchanger. The total heat and mass transfer increase and the overall irreversibility in the system decreases with an increase in both width and effective length.

Figure 17(a) shows that increasing the length of the module results in a large increase in GOR. With the flow characteristics and mass flow ratios unaltered, the increase is predominantly owing to better usage of the heat in the feed stream. With increase

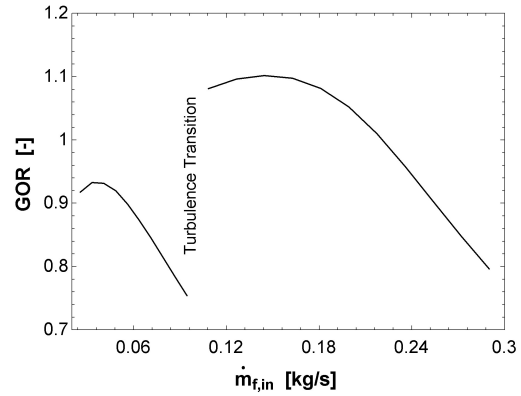

(a) Feed side. Discontinuity due to transition to turbulence

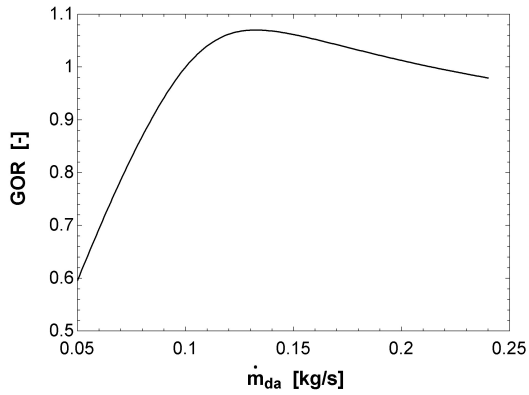

(b) Air side

FIGURE 14. GOR DEPENDENCE ON MASS FLOW RATES

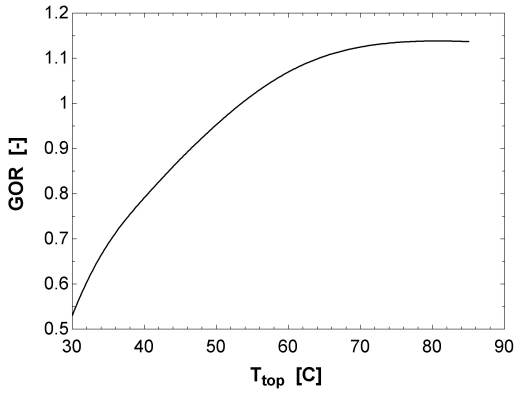

FIGURE 15. GOR DEPENDENCE ON CYCLE TOP TEMPERATURE

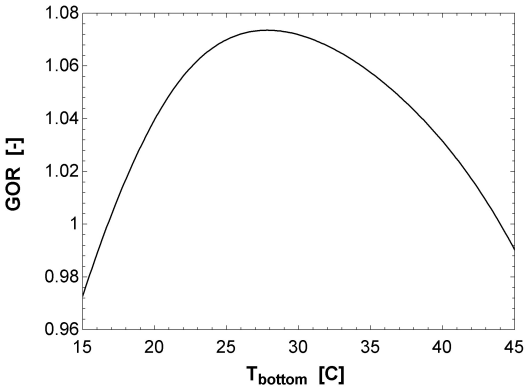

FIGURE 16. GOR DEPENDENCE OF CYCLE BOTTOM TEMPERATURE

in length, $T_{f,out}$ decreases and the mass transfer occurs over a smaller Δp_v.

In Figure 17(b), the gap in the graph corresponds to a change of feed flow regime to laminar as the cross sectional area increases with increase in width. The GOR increase is observed over a smaller range in the case of width as compared to length. This is because of the other being held constant. When the width is increased to 3 m, the length is held constant at 12 m resulting in an overall membrane area of 36 m^2. On the other hand, to reach the same membrane area with a width of 0.125 m, the lenght must be 144 m. Note that at an effective length of 144 m, the GOR achieved is higher than at width of 3 m though the overall membrane area is the same. This is because an increase in length does not affect the flow regime in the module and the feed and air Reynolds numbers remain the same ($Re_f \approx 5000, Re_a \approx 4.4 \times 10^4$). On the other hand, the Reynolds numbers and hence heat and mass transfer coefficients of both streams reduce with an increase in width. In a real system one would have to pay for the increased GOR in the longer module in the form of a much larger pressure drop and hence pumping power, compared to the wider module which has a slightly lower GOR.

The effect of the depth of the two channels is illustrated in Figure 18. The effect of increasing d is similar for both the streams. The membrane area remains unaltered and the only effect is on cross sectional area and therefore on the transport processes and boundary layers in the two streams. Correspondingly, the change in GOR over the range of d_f and d_a is smaller than in the case of the other dimensions. An increase in depth of the channel leads to higher boundary layer resistances and therefore smaller GOR. Figures 18(a) and 18(b) suggest that polarizations in both streams are significant. The temperature polarization in the feed stream and concentration polarization in the air stream have maximum impact since they directly affect the mass transfer

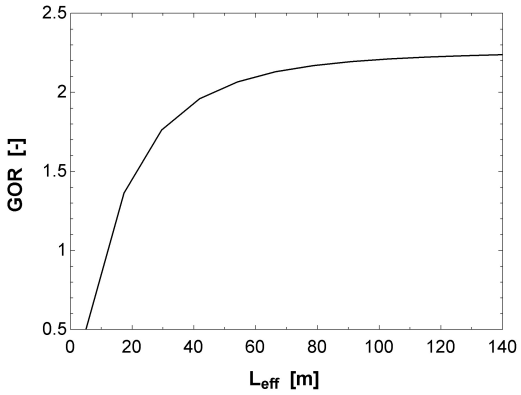

(a) Effective length

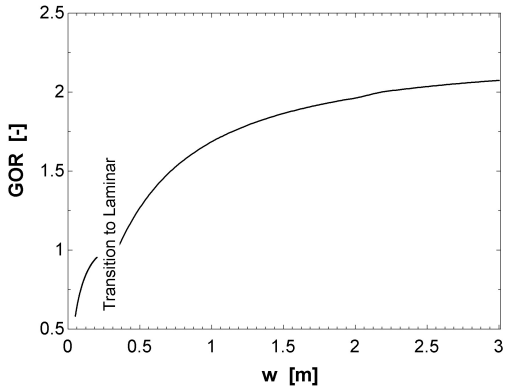

(b) Width

FIGURE 17. GOR DEPENDENCE ON LENGTH AND WIDTH

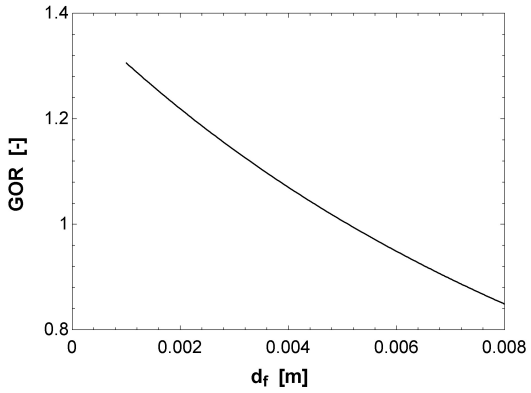

(a) Feed side

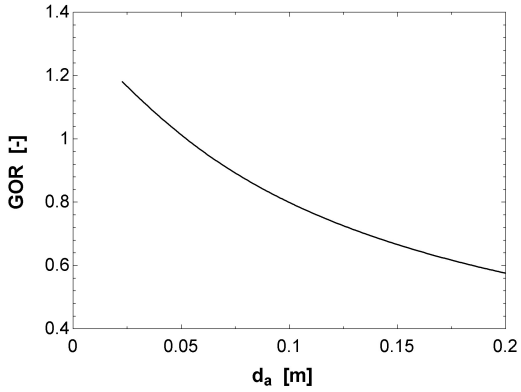

(b) Air side

FIGURE 18. GOR DEPENDENCE ON CHANNEL DEPTH

driving force by reducing the vapor pressure difference substantially. The concentration polarization on the feed side can have a significant effect too, especially under laminar flow conditions.

5.4 Dehumidifer effectiveness

MSBCDH effectiveness increases with number of stages. The number of stages determines the pressure drop through the system and the cost. The marginal gains in GOR with increase in the number of stages of the dehumidifier is presented in Fig. 19.

5.5 Membrane properties

The B value of the membrane directly influences the flux in MD processes. With higher B giving rise to higher flux, one could use smaller devices. In other words, if the membrane area is held constant and the membrane permeability is increased, we can expect to see an increase in efficiency as shown in Fig. 20. It should be noted that higher permeability alone does not guarantee good thermal efficiency (GOR vs. B graph plateaus beyond a point). While high permeability membranes will help, they are not a substitute for thermodynamic analysis and cycle design.

5.6 Further improvements

In the preceding sections, the effect of each independent variable was studied keeping other parameters fixed. This yields a GOR just over 2 with large enough membrane area (≈ 36 m^2). Further improvements to GOR are possible when all the independent variables are allowed to change. For example, Fig. 21 shows the effect of feed mass flow rate on GOR when the module effective length is set as 60 m. The maximum GOR attained is close to 2.6 in this case.

6 CONCLUSIONS

A one-dimensional numerical model of the heat and mass transfer processes occurring in a SGMD module is developed.

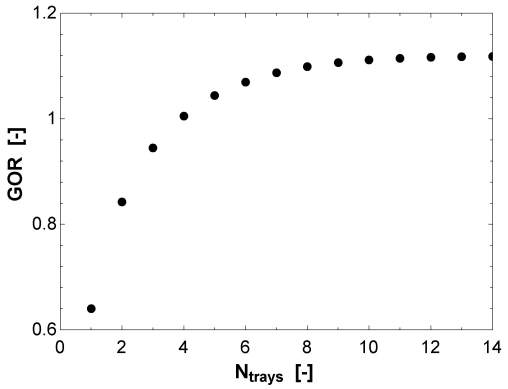

FIGURE 19. EFFECT OF NUMBER OF BCDH STAGES

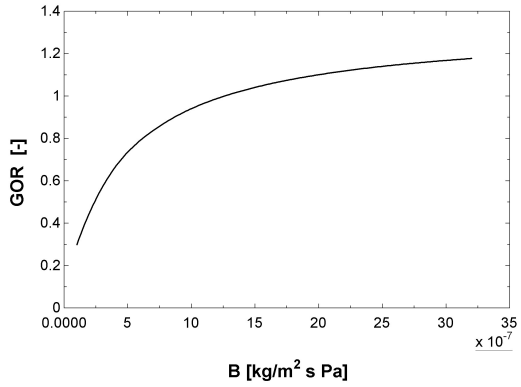

FIGURE 20. EFFECT OF MEMBRANE PERMEABILITY

The model can take in both saturated and unsaturated air as input and the process path is evaluated using the membrane distillation coefficient B. Entropy generation within the SGMD module is studied with respect to changes in the system variables.

The model has been used to study the energy efficiency of the SGMD based desalination cycle using a multistage bubble column dehumidifier to recover pure water. Entropy generation in the dehumidifier is found to be important, often competing with the SGMD module in deciding the optimum operating conditions.

The boundary layer resistances and associated temperature/concentration polarizations are found to have a significant impact on reducing thermal efficiency. Improvements in mixing within the streams such as the use of suitable spacers of baffles can lead to further improvements in efficiency.

This model can be a useful tool for designing optimal desalination cycles under a set of design constraints. The effect of each independent variable on GOR was studied. For a longer module,

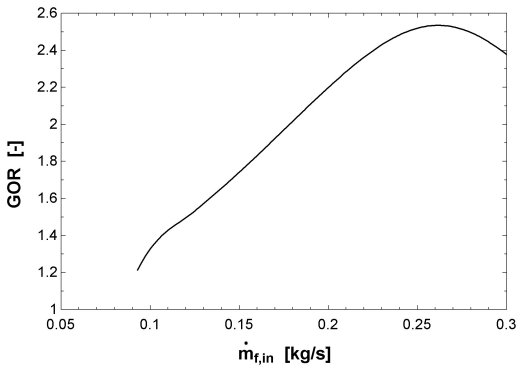

FIGURE 21. GOR VS. FEED MASS FLOW RATE. $L = 60$ m

a maximum GOR in excess of 2.5 is observed with changing feed mass flow rate. Now that the effect of each individual process parameter is understood, further optimization is possible to look for operating conditions that yield global maximum GOR.

ACKNOWLEDGMENT

This work was funded by the Cooperative Agreement Between the Masdar Institute of Science and Technology (Masdar University), Abu Dhabi, UAE and the Massachusetts Institute of Technology (MIT), Cambridge, MA, USA, Reference No. 02/MI/MI/CP/11/07633/GEN/G/00.

REFERENCES

[1] Alkhudhiri, A., Darwish, N., and Hilal, N., 2012. "Membrane distillation: A comprehensive review". *Desalination,* ***287***, Feb., pp. 2–18.

[2] Martinez-Diez, L., and Vazquez-Gonzalez, M., 1999. "Temperature and concentration polarization in membrane distillation of aqueous salt solutions". *Journal of Membrane Science,* ***156***(2), pp. 265 – 273.

[3] El-Bourawi, M., Ding, Z., Ma, R., and Khayet, M., 2006. "A framework for better understanding membrane distillation separation process". *Journal of Membrane Science,* ***285***(1-2), Nov., pp. 4–29.

[4] Khayet, M., and Matsuura, T., 2011. *Membrane Distillation Principles and Applications*. Elsevier.

[5] Narayan, G. P., Sharqawy, M. H., Lam, S., Das, S. K., and Lienhard V, J. H., 2012. "Bubble columns for condensation at high concentrations of non condensable gas: Heat transfer model and experiments". *AIChE Journal,* ***59***(5), pp. 1780–1790.

[6] Summers, E. K., Arafat, H. A., and Lienhard, J. H., 2012. "Energy efficiency comparison of single-stage membrane

distillation (MD) desalination cycles in different configurations". *Desalination,* ***290***, Mar., pp. 54–66.

[7] S.A.Klein. Engineering equation solver version 9.

[8] Hyland, R., and Wexler, A., 1983. "Formulations for the thermodynamic properties of the saturated phases of H2O from 173.15K to 473.15K". *ASHRAE Transactions (Part 2A)*.

[9] Pruss, A., and Wagner, W., 2002. "The IAPWS formulation 1995 for the thermodynamic properties of ordinary water substance for general and scientific use". *Journal of Physical and Chemical Reference Data,* ***2***, pp. 387–535.

[10] Khayet, M., Godino, P., and Mengual, J. I., 2000. "Theory and experiments on sweeping gas membrane distillation". pp. 261–272.

[11] Khayet, M., Godino, M. P., and Mengual, J. I., 2002. "Thermal boundary layers in sweeping gas membrane distillation processes". *AIChE Journal,* ***48***(7), July, pp. 1488–1497.

[12] Charfi, K., Khayet, M., and Safi, M., 2010. "Numerical simulation and experimental studies on heat and mass transfer using sweeping gas membrane distillation". *Desalination,* ***259***(1-3), Sept., pp. 84–96.

[13] Lienhard V, J. H., and Lienhard IV, J. H., 2011. *A Heat Transfer Textbook Fourth Edition*. Dover Publications, Inc.

[14] Tow, E. W., and Linhard V, J. H., 2013. "Heat Flux and Effectiveness in Bubble Column Dehumidifiers". In Proceedings of the 2013 IDA World Congress on Desalination and Water Reuse, IDA.

[15] Mistry, K. H., McGovern, R. K., Thiel, G. P., Summers, E. K., Zubair, S. M., and Lienhard V, J. H., 2011. "Entropy Generation Analysis of Desalination Technologies". *Entropy,* ***13***(10), Sept., pp. 1829–1864.

[16] Narayan, G. P., Lienhard V, J. H., and Zubair, S. M., 2010. "Entropy generation minimization of combined heat and mass transfer devices". *International Journal of Thermal Sciences,* ***49***(10), pp. 2057 – 2066.